

A Numerical Method for the Simulation of Free Surface Flows with Surface Tension

Alexandre Caboussat¹

*University of Houston, Department of Mathematics
4800 Calhoun Rd, Houston, Texas 77204-3008, USA*

Abstract

A numerical model for the simulation of three-dimensional liquid-gas flows with free surfaces and surface tension is presented. The incompressible Navier-Stokes equations are assumed to hold in the liquid domain, while the gas pressure is assumed to be constant in each connected component of the gas domain and to follow the ideal gas law. The surface tension effects are imposed as a normal force on the interface.

An implicit splitting scheme is used to decouple the physical phenomena. Given the curvature of the liquid-gas interface, the method described in [5] is used to track the liquid domain and compute the velocity and pressure in the liquid and the pressure in the gas domain. Then the surface tension effects are added. A variational method for the computation of the curvature is presented by smoothing the characteristic function of the liquid domain and using a finite element unstructured mesh.

The model is validated and numerical results in two and three space dimensions are presented in the frame of bubbles and/or droplets flows.

Key words: Surface Tension, Volume of Fluid, Free Surface, Curvature

1 Introduction

Free surface flows appear in many physical situations. Surface tension effects are not always relevant, especially when the Reynolds number is large, but

* Corresponding author: Phone: +1 713 743 3491 / Fax : +1 713 743 3505

Email address: caboussat@math.uh.edu (Alexandre Caboussat).

¹ Supported by the Swiss National Science Foundation, Grant PBEL2-103152

they become very important when we deal with quasi-stationary bubbles or droplets, see *e.g.* [30], crashing droplets of water [10,11,28], rising bubbles [31], viscoelastic flows [26] or wave propagation [9].

In this article, we focus on the simulation of two-phase flows, namely an incompressible liquid and a compressible gas. The velocity and pressure are modeled in the liquid, while only the pressure is considered in the gas domain. The aim of this article is to extend the model proposed in [5] by adding the surface tension effects.

Many methods exist for the modeling of surface tension effects on the liquid-gas interface (see [3,23] for instance for a review). The continuum surface force model (CSF) [3,7,22,32] is used here. Contact angles (*i.e.* triple-points for instance) are not modeled. The surface tension effects are expressed by a normal force on the free surface, so that the equilibrium relation on the liquid-gas interface is

$$-p\mathbf{n} + 2\mu\mathbf{D}(\mathbf{v})\mathbf{n} = -P\mathbf{n} + \sigma\kappa\mathbf{n} ,$$

where κ is the curvature of the liquid-gas interface, \mathbf{n} is the normal vector to the interface (oriented towards the gas domain) and σ is a constant coefficient which depends on the physical properties of both, the liquid and the gas. The pressure in the liquid is here denoted by p , while P denotes the pressure in the gas. The velocity of the liquid is denoted by \mathbf{v} and $D(\mathbf{v})$ is the rate of stress tensor. Dynamical effects in the gas domain are neglected.

The characteristic function of the liquid domain is considered and a volume-of-fluid method is used. An implicit time splitting scheme extracted from [5,13,14] permits to decouple the various physical phenomena. Two advection problems are first solved on a structured grid and then the gas pressure, the surface tension effects and a diffusion problem are solved on an unstructured finite element mesh. We focus here on the computation of the surface tension effects. The curvature can be computed by approximating the second derivatives of the volume fraction of liquid [19], by computing the volume fraction of a sphere which lies on one side of the interface [4], or with geometric considerations [18]. Generally the computation of the curvature is carried out on a structured grid and need a very accurate reconstruction of the interface [1,21]. A method for the computation of surface tension effects is proposed here on an unstructured finite element mesh, independently of the space dimension (see also [27] for a similar approach).

The curvature κ is defined by the divergence of the normal vector to the interface [17,25]

$$\kappa = \operatorname{div}\mathbf{n} .$$

The very well-known drawback of the volume-of-fluid method is the lack of regularity of the characteristic function of the liquid domain φ across the interface. In order to compute its derivatives, φ is first convoluted with a smooth kernel [21,32]. An artificial curvature is then obtained at each grid point of the unstructured mesh by computing the projection of the divergence of the normal vector in the L^2 -sense on the piecewise linear finite element space based on an unstructured mesh. The surface tension force is then applied at the grid points lying on the numerical approximation of the liquid-gas interface.

The structure of this article is as follows. In Sect. 2, the numerical model for the simulation of a two-phase flow involving an incompressible liquid and a compressible gas is described. In Sect. 3, a time splitting scheme is presented, which permits to decouple the computation of the surface tension effects from the other physical phenomena. The space discretization is detailed in Sect. 4. Finally, in Sect. 5, convergence results are obtained for the approximation of the curvature and numerical simulations are presented in two and three dimensions to illustrate the efficiency of our approach in various situations.

2 The Mathematical Model

The numerical simulation of this liquid-gas free surface flow without taking into account the surface tension effects has been described in [5,13,14]. The model presented in this section is an extension of the one described in [5] in which the surface tension effects are taken here into account by adding a normal force on the liquid-gas interface.

Let Λ be a cavity of \mathbb{R}^d , $d = 2, 3$ in which the fluid must be confined, and let $T > 0$ be the final time of simulation. For any given time t , let Ω_t be the domain occupied by the liquid and let Γ_t be the free surface defined by $\partial\Omega_t \setminus \partial\Lambda$. The notations are reported in Fig. 1 in the frame of a two-dimensional situation, namely the rising of an air bubble in water under gravity forces.

Let Q_T denote the space-time domain containing the liquid, that is $Q_T = \{(x, t) : x \in \Omega_t, 0 < t < T\}$. In the liquid region, the velocity field $\mathbf{v} : Q_T \rightarrow \mathbb{R}^d$ and the pressure field $p : Q_T \rightarrow \mathbb{R}$ are assumed to satisfy the time-dependent, incompressible Navier-Stokes equations, that is

$$\rho \frac{\partial \mathbf{v}}{\partial t} + \rho(\mathbf{v} \cdot \nabla) \mathbf{v} - 2 \operatorname{div}(\mu \mathbf{D}(\mathbf{v})) + \nabla p = \mathbf{f} \quad \text{in } Q_T, \quad (1)$$

$$\operatorname{div} \mathbf{v} = 0 \quad \text{in } Q_T. \quad (2)$$

Here $\mathbf{D}(\mathbf{v}) = \frac{1}{2}(\nabla \mathbf{v} + \nabla \mathbf{v}^T)$ is the rate of deformation tensor, ρ the constant density, μ the viscosity and \mathbf{f} denotes the external forces.

Let $\varphi : \Lambda \times (0, T) \rightarrow \mathbb{R}$ be the characteristic function of the liquid domain Q_T . The function φ equals one if liquid is present, zero if it is not. In order to describe the kinematics of the free surface, φ must satisfy (in a weak sense):

$$\frac{\partial \varphi}{\partial t} + \mathbf{v} \cdot \nabla \varphi = 0 \quad \text{in } Q_T . \quad (3)$$

In the gas region, the velocity is disregarded, so that the only unknown is the pressure. At each time t , the pressure $P(t) : \Lambda \setminus \Omega_t \rightarrow \mathbb{R}$ in the gas is assumed to be piecewise constant in each bubble of gas, that is in each connected component of the gas domain. The gas is supposed to be an ideal gas at constant temperature. Let us denote by $k(t)$ the total number of bubbles of gas at time $t \in (0, T)$ and by $B_i(t)$ the bubble number i . The law of ideal gases is assumed to hold in each bubble, which implies

$$P_i(t)V_i(t) = \text{constant in bubble number } i , \quad (4)$$

The velocity in the gas is thus disregarded and the connected components of the gas domain have to be tracked at each time step. In most situations and when the time step is small enough, three situations may appear between two time steps at different locations in the process: first, a single bubble may stay a single bubble; then a bubble may split into two bubbles and, finally, two bubbles may merge into one. In these three cases, the pressure at time $t + \tau$ may be computed by taking into account the conservation of number of molecules in the bubbles between the time t and $t + \tau$. A detailed discussion may be found in [5].

The initial conditions are the following. At initial time, the characteristic function of the liquid domain φ is given, which defines the initial liquid region $\Omega_0 = \{x \in \Lambda : \varphi(x, 0) = 1\}$. The initial velocity field \mathbf{v} is then prescribed in Ω_0 . The initial gas pressure field is prescribed in $\Lambda \setminus \Omega_0$ and is assumed to be constant in each bubble of gas existing at initial time.

The boundary conditions for the velocity field are the following. On the boundary of the liquid region being in contact with the walls (that is to say the boundary of Λ , see Fig. 1), Dirichlet or slip boundary conditions are enforced, see [13,14]. On the free surface Γ_t , tangential and capillary forces are neglected in this article, since creeping flows at very low Reynolds number are not considered here. Thus the forces acting on the free surface are the normal forces due to the gas pressure and the surface tension effects. At given time t , let $\kappa(x, t)$ be the curvature of the interface Γ_t at point x . The following equilibrium relation is then satisfied on the liquid-gas interface:

$$-p\mathbf{n} + 2\mu\mathbf{D}(\mathbf{v})\mathbf{n} = -P\mathbf{n} + \sigma\kappa\mathbf{n} \quad \text{on } \Gamma_t, \quad t \in (0, T) , \quad (5)$$

where \mathbf{n} is the unit normal of the liquid-gas free surface oriented toward the gas domain, P is the pressure in the gas, κ is the local curvature of the interface and σ is a constant surface tension coefficient which depends on both media on each side of the interface (namely the liquid and the gas). By definition, the curvature $\kappa(x, t)$ is supposed to be negative if the center of the osculating circle of the interface at point x is on the liquid side of the interface (see [6] for a similar convention).

For example, consider the situation of Fig. 1, namely the rising of a single bubble of air initially at the bottom of a glass of water (the numerical experiment is described in Sect. 5). When the bubble rises, a force (5) is exerted on the interface; the first contribution of this force is a normal force induced by the pressure of the trapped gas which prevents the bubble from collapsing, while the second contribution is due to the surface tension effects.

The mathematical description of our model is now completed. The model unknowns are the characteristic function φ in the whole cavity, the velocity \mathbf{v} and pressure p in the liquid domain, the connected components of the gas domain (bubbles), the pressure P in the gas domain and the curvature κ and the normal vector \mathbf{n} on the liquid-gas interface. These unknowns satisfy equations (1), (2), (3) and (4) with the boundary condition (5) on the free surface Γ_t .

3 A Time Splitting Algorithm

In [13,14], an implicit, order one splitting algorithm was used to solve the problem (1)-(5), with $P = 0$ and $\sigma = 0$, by decoupling the advection phenomena from the diffusion phenomena. In [5], the splitting algorithm has been extended by taking into account the gas pressure P with (4). In this paper, an extended splitting algorithm is proposed to aggregate the surface tension effects in (5).

Let $0 = t^0 < t^1 < t^2 < \dots < t^N = T$ be a subdivision of the time interval $[0, T]$ and $\tau^n = t^{n+1} - t^n$ the n -th time step, $n = 1, 2, \dots, N$, τ the largest time step.

Let $\varphi^n, \mathbf{v}^n, \Omega^n, k^n, P^n, B_i^n, i = 1, 2, \dots, k^n$ and κ^n, \mathbf{n}^n be approximations of $\varphi, \mathbf{v}, \Omega, k, P, B_i, i = 1, 2, \dots, k$ and κ, \mathbf{n} respectively at time t^n . Then the approximations $\varphi^{n+1}, \mathbf{v}^{n+1}, \Omega^{n+1}, k^{n+1}, P^{n+1}, B_i^{n+1}, i = 1, 2, \dots, k^{n+1}$ and $\kappa^{n+1}, \mathbf{n}^{n+1}$ at time t^{n+1} are computed by means of an implicit splitting algorithm, as illustrated in Fig. 2.

First two advection problems are solved, leading to a prediction of the new

velocity $\mathbf{v}^{n+1/2}$ together with the new approximation of the characteristic function of the liquid domain φ^{n+1} . This allows to determine the new liquid domain Ω^{n+1} , the new gas domain $\Lambda \setminus \Omega^{n+1}$ and the new liquid-gas interface Γ^{n+1} . Then the connected components of gas (bubbles) B_i^{n+1} , $i = 1, \dots, k^{n+1}$ are tracked with a procedure we sketch in the following and the constant pressure P_i^{n+1} in each bubble B_i^{n+1} is computed. Then an approximation of the curvature κ^{n+1} is obtained on the interface Γ^{n+1} together with the normal vector \mathbf{n}^{n+1} . Finally, a generalized Stokes problem is solved on Ω^{n+1} with boundary condition (5) on Γ^{n+1} and Dirichlet or slip conditions on the boundary of the cavity Λ and the correction of the velocity \mathbf{v}^{n+1} and the pressure p^{n+1} in the liquid are obtained.

The advection step consists in solving between the times t^n and t^{n+1} the two advection problems:

$$\frac{\partial \mathbf{v}}{\partial t} + (\mathbf{v} \cdot \nabla) \mathbf{v} = 0 \quad , \quad (6)$$

$$\frac{\partial \varphi}{\partial t} + \mathbf{v} \cdot \nabla \varphi = 0 \quad , \quad (7)$$

with initial conditions given by the values of the functions \mathbf{v} and φ at time t^n . This step is solved with a forward characteristics method, *i.e.* the prediction of the velocity and the new approximation of the characteristic function are given by $\mathbf{v}^{n+1/2}(x + \tau^n \mathbf{v}^n(x)) = \mathbf{v}^n(x)$ and $\varphi^{n+1}(x + \tau^n \mathbf{v}^n(x)) = \varphi^n(x)$, for all $x \in \Omega^n$. The domain Ω^{n+1} is then defined as the set of points such that φ^{n+1} equals one.

Given the liquid domain Ω^{n+1} , the bubbles of gas B_i^{n+1} are then recognized with a numbering algorithm. This step is widely detailed in [5]. The key point is to find the bubbles number k^{n+1} and the bubbles B_i^{n+1} , $i = 1, \dots, k^{n+1}$. The algorithm for detecting a connected component of the gas domain is the following. At each time step, given a point P outside the liquid domain $\overline{\Omega^{n+1}}$, we first search for a function u such that $-\Delta u = \delta_P$ in the domain Θ^{n+1} initially defined by $\Lambda \setminus \Omega^{n+1}$, with $u = 0$ on $\Lambda \setminus \Theta^{n+1}$ and u continuous, *i.e.*: find $u : \Lambda \rightarrow \mathbb{R}$ which satisfies:

$$\begin{cases} -\Delta u = \delta_P, & \text{in } \Theta^{n+1} \quad , \\ u = 0, & \text{in } \Lambda \setminus \Theta^{n+1} \quad , \\ [u] = 0, & \text{on } \partial\Theta^{n+1} \quad , \end{cases} \quad (8)$$

Since the solution u to this problem is strictly positive in the connected component of Θ^{n+1} containing the point P and is vanishing outside, the first bubble is found. The procedure is then repeated to recognize one connected

component after the other by removing the previous connected component from Θ^{n+1} and choosing another point P . Details may be found in [5].

Then the curvature of the free surface Γ^{n+1} and the normal vector \mathbf{n}^{n+1} are computed. Since the characteristic function φ^{n+1} is not regular across the interface, it is first mollified in order to obtain a smooth function $\tilde{\varphi}^{n+1}$ such that the liquid-gas interface is given by the level line $\{x \in \Lambda : \tilde{\varphi}^{n+1}(x) = 1/2\}$, with $\tilde{\varphi}^{n+1} < 1/2$ in the gas domain and $\tilde{\varphi}^{n+1} > 1/2$ in the liquid domain. At each time step, the normal vector \mathbf{n}^{n+1} directed outside the liquid domain towards the gas domain and the curvature κ^{n+1} on the liquid-gas interface are then given by:

$$\mathbf{n}^{n+1} = -\frac{\nabla \tilde{\varphi}^{n+1}}{\|\nabla \tilde{\varphi}^{n+1}\|}, \quad \kappa^{n+1} = \operatorname{div} \mathbf{n}^{n+1} = -\operatorname{div} \frac{\nabla \tilde{\varphi}^{n+1}}{\|\nabla \tilde{\varphi}^{n+1}\|}, \quad (9)$$

where $\|\cdot\|$ denotes the Euclidean norm in \mathbb{R}^d , $d = 2, 3$, see *e.g.* [17,25].

Let us turn first to the smoothing of the characteristic function φ^{n+1} . Let $K_\varepsilon(x)$ be a *kernel* function, *i.e.* which has a compact support and is radially-symmetric, monotonically decreasing with respect to $r = \|x\|$ and normalized. The convolution of φ^{n+1} with K_ε leads to a smoothed volume fraction of liquid $\tilde{\varphi}^{n+1}$ defined by:

$$\tilde{\varphi}^{n+1}(x) = \int_{\Lambda} \varphi^{n+1}(y) K_\varepsilon(x-y) dy, \quad \forall x \in \Lambda. \quad (10)$$

The kernel used in our algorithm has been proposed in [32] and is given by:

$$K_\varepsilon(x) = \begin{cases} C \left(1 - \left(\frac{\|x\|}{\varepsilon}\right)^2\right)^4, & \text{if } \|x\| \leq \varepsilon, \\ 0, & \text{otherwise} \end{cases} \quad (11)$$

where C is a normalization coefficient, depending on the space dimension. Hence the normal vector \mathbf{n}^{n+1} and the curvature κ^{n+1} can be approximated by (9). Observe that the first derivatives of $\tilde{\varphi}^{n+1}$ may even be obtained with an exact expression:

$$\frac{\partial \tilde{\varphi}^{n+1}}{\partial x_i}(x) = \int_{\Lambda} \varphi^{n+1}(y) \frac{\partial K_\varepsilon}{\partial x_i}(x-y) dy, \quad i = 1, \dots, d. \quad (12)$$

where $d = 2, 3$ is the space dimension of the problem.

Finally, the diffusion step consists in solving a generalized Stokes problem on the domain Ω^{n+1} using the predicted velocity $\mathbf{v}^{n+1/2}$ and the boundary condition (5). The following implicit Euler scheme is used:

$$\rho \frac{\mathbf{v}^{n+1} - \mathbf{v}^{n+1/2}}{\tau^n} - 2\text{div}(\mu \mathbf{D}(\mathbf{v}^{n+1})) + \nabla p^{n+1} = \mathbf{f} \quad \text{in } \Omega^{n+1}, \quad (13)$$

$$\text{div } \mathbf{v}^{n+1} = 0 \quad \text{in } \Omega^{n+1}, \quad (14)$$

The boundary conditions on the free surface between the liquid and the bubble number i are given by (5). The weak formulation corresponding to (13) (14) and (5) therefore consists in finding \mathbf{v}^{n+1} and p^{n+1} such that \mathbf{v}^{n+1} satisfies the essential boundary conditions on the boundary of the cavity Λ and

$$\begin{aligned} & \int_{\Omega^{n+1}} \frac{\mathbf{v}^{n+1} - \mathbf{v}^{n+1/2}}{\tau^n} \mathbf{w} dx + 2\mu \int_{\Omega^{n+1}} D(\mathbf{v}^{n+1}) : D(\mathbf{w}) dx \\ & - \int_{\Omega^{n+1}} p^{n+1} \text{div } \mathbf{w} dx - \int_{\Omega^{n+1}} \mathbf{f} \mathbf{w} dx - \int_{\Omega^{n+1}} \text{div } \mathbf{v}^{n+1} q dx \\ & + \int_{\Gamma^{n+1}} (P^{n+1} - \sigma \kappa^{n+1}) \mathbf{n}^{n+1} \mathbf{w} dS = 0, \end{aligned} \quad (15)$$

for all (\mathbf{w}, q) compatible with the essential boundary conditions on the boundary of Ω^{n+1} .

4 The Space Discretization

A two-grids method is used for the spatial discretization, see Fig. 3. In particular, a regular grid of small cells is used to solve the advection step, while the computations of the gas pressure, surface tension effects and diffusion step are performed on an unstructured finite element mesh.

The advection step is solved on the fine structured grid of small cells with a forward characteristics method. Assume that the grid is made out of cubic cells of size h , each cell being labeled by indices (ijk) . Let φ_{ijk}^n and \mathbf{v}_{ijk}^n be the approximate value of φ and \mathbf{v} at the center of cell number (ijk) at time t^n . The unknown φ_{ijk}^n is the so-called volume fraction of liquid in the cell (ijk) , see [1]. This numerical approximation of the characteristic function φ at time t^n is then piecewise constant on each cell of the structured grid. The advection step in the cell (ijk) consists in advecting φ_{ijk}^n and \mathbf{v}_{ijk}^n by $\tau^n \mathbf{v}_{ijk}^n$ and then projecting the values on the structured grid. An example of cell advection and projection is presented in Fig. 4 in two space dimensions.

In order to enhance the quality of the volume fraction of liquid, post-processing procedures have been implemented. In particular, a variation of the SLIC algorithm [16] allows to reduce the numerical diffusion on the regular grid of small cells by pushing the liquid on the sides of the cell before advecting it and projecting on the grid. Precise examples and detailed description are given in [13,14] for the two- and three-dimensional cases. A post-processing technique which allows to produce new values φ_{ijk}^{n+1} which are between zero and one is also implemented and detailed in [5], where the efficiency of these procedures for stretching flows with prescribed velocity is also shown.

Once values φ_{ijk}^{n+1} and $\mathbf{v}_{ijk}^{n+1/2}$ have been computed on the cells, values of the fraction of liquid φ_P^{n+1} and of the velocity field $\mathbf{v}_P^{n+1/2}$ are computed at the nodes P of the finite element mesh by multi-grids restriction methods: for any vertex P of the finite element mesh let ψ_P be the corresponding basis function (i.e. the continuous, piecewise linear function having value one at P , zero at the other vertices of the finite element mesh). We consider all the tetrahedrons K containing vertex P and all the cells (ijk) having center of mass C_{ijk} contained in these tetrahedrons. Then, φ_P^{n+1} , the volume fraction of liquid at vertex P and time t^{n+1} is computed using the following weighted sum:

$$\varphi_P^{n+1} = \frac{\sum_{\substack{K \\ P \in K}} \sum_{\substack{ijk \\ C_{ijk} \in K}} \psi_P(C_{ijk}) \varphi_{ijk}^{n+1}}{\sum_{\substack{K \\ P \in K}} \sum_{\substack{ijk \\ C_{ijk} \in K}} \psi_P(C_{ijk})}.$$

The same kind of formula is used to obtain the predicted velocity $\mathbf{v}^{n+1/2}$ at the vertices of the finite element mesh. When these values are available at the vertices of the finite element mesh, the liquid region is defined as follows. An element of the finite element mesh is said to be liquid if (at least) one of its vertices P has a value $\varphi_P^{n+1} > 0.5$. The computational domain used for solving (15) is then defined to be the union of all liquid elements.

The numbering of the bubbles of gas requires to solving Poisson problems (8). The Poisson problems are solved on the finite element unstructured mesh, using piecewise linear finite elements. Once the connected components of the gas domain are recognized, a constant pressure is computed by using the law of ideal gases (4). The volume of each bubble of gas is computed by the sum of the volumes of the elements of the finite element mesh belonging to the bubble, weighted by the mean volume fraction of liquid. Details may be found in [5].

An approximation of the curvature of the interface can be computed on the structured grid of small cells with finite differences schemes for instance. Sev-

eral methods may be found in [10,22] for instance. Nevertheless, these methods need a very accurate reconstruction of the interface with sophisticated algorithms such as PLIC schemes for instance [1]. On the other hand the method proposed here uses a formulation on the finite element unstructured mesh.

Let \mathcal{T}_h be the triangulation of the cavity Λ , Ω_h^{n+1} be the approximation of the liquid domain composed by elements K in \mathcal{T}_h and Γ_h^{n+1} the approximation of Γ^{n+1} . Let ψ_{P_j} be the basis functions of the piecewise linear finite element space associated to each node P_j , $j = 1, \dots, N$ in the cavity. Finally, let the piecewise linear finite elements space be denoted by $X_h^1(\Lambda)$.

Let $\tilde{\varphi}_h^{n+1}, \varphi_h^{n+1}$ be the approximations of $\tilde{\varphi}^{n+1}, \varphi^{n+1}$ in $X_h^1(\Lambda)$. The numerical integration of (10) can either be made on the regular grid of small cells or on the finite element mesh; for memory purposes, it is performed on the finite element mesh, that is:

$$\tilde{\varphi}_h^{n+1}(P_i) = \sum_{K \in \mathcal{T}_h} \frac{1}{d+1} |K| \sum_{P_j \in K} \varphi_h^{n+1}(P_j) K_\varepsilon(P_j - P_i), \quad i = 1, \dots, N, \quad (16)$$

where $d = 2, 3$ is the space dimension of the problem and $|K|$ denotes the surface (resp. volume) of the element K . This leads to an approximation of the smoothed volume fraction of liquid for each grid point P_i of \mathcal{T}_h .

The procedure detailed hereafter gives a natural expression of the curvature (9) on the finite element mesh grid points in a variational framework and is not CPU time consuming.

The normal vector \mathbf{n}_h^{n+1} is given by (9) (12) (with φ^{n+1} replaced by φ_h^{n+1}) at each grid point P_j . The approximation of the curvature κ^{n+1} in (9) is denoted by κ_h^{n+1} and computed by the L^2 -projection on $X_h^1(\Lambda)$ of the divergence of \mathbf{n}_h^{n+1} with *mass lumping*. The projection reads:

$$\int_{\Lambda} R_h(\kappa_h^{n+1} \psi_{P_j}) dx = \int_{\Lambda} -\operatorname{div} \frac{\nabla \tilde{\varphi}_h^{n+1}}{\|\nabla \tilde{\varphi}_h^{n+1}\|} \psi_{P_j} dx, \quad \forall j = 1, \dots, N. \quad (17)$$

where R_h denotes the Lagrange interpolant on $X_h^1(\Lambda)$. Relationship (17) leads to:

$$\begin{aligned} \kappa_h^{n+1}(P_j) = \frac{d+1}{|\Omega_j|} & \left[\sum_{K \in \mathcal{T}_h} |K| \left(\frac{1}{d+1} \sum_{P_i \in K} \frac{\nabla \tilde{\varphi}_h^{n+1}(P_i)}{\|\nabla \tilde{\varphi}_h^{n+1}\|} \right) \nabla \psi_{P_j} \Big|_K \right. \\ & \left. - \sum_{\substack{\partial K \subset \partial \Lambda \\ P_j \in K}} \frac{1}{d} \frac{\nabla \tilde{\varphi}_h^{n+1}(P_j)}{\|\nabla \tilde{\varphi}_h^{n+1}\|} \mathbf{n}_{\Lambda, h}(P_j) |\partial K| \right], \end{aligned} \quad (18)$$

where $|\Omega_j| = \sum_{K, P_j \in K} |K|$ and $\mathbf{n}_{\Lambda, h}$ denotes the approximation of the external normal vector to the cavity Λ .

One artificial value of the curvature is thus given by the piecewise linear function κ_h^{n+1} defined by (18) in the whole cavity, that is for each level line of the smoothed volume fraction of liquid $\tilde{\varphi}_h^{n+1}$. The restriction of κ_h^{n+1} to the nodes P_j lying on Γ_h^{n+1} is used in (5).

Finally the diffusion step consists in solving the Stokes problem (15). Let \mathbf{v}_h^{n+1} (resp. p_h^{n+1}) be the piecewise linear approximation of \mathbf{v}^{n+1} (resp. p^{n+1}). The Stokes problem is solved with stabilized $\mathbb{P}_1 - \mathbb{P}_1$ finite elements (Galerkin Least Squares method) and consists in finding the velocity \mathbf{v}_h^{n+1} and pressure p_h^{n+1} such that:

$$\begin{aligned} & \int_{\Omega_h^{n+1}} \frac{\mathbf{v}_h^{n+1} - \mathbf{v}_h^{n+1/2}}{\tau^n} \mathbf{w} dx + 2\mu \int_{\Omega_h^{n+1}} D(\mathbf{v}_h^{n+1}) : D(\mathbf{w}) dx - \int_{\Omega_h^{n+1}} \mathbf{f} \mathbf{w} dx \\ & - \int_{\Omega_h^{n+1}} p_h^{n+1} \operatorname{div} \mathbf{w} dx + \int_{\Gamma_h^{n+1}} (P^{n+1} - \sigma \kappa_h^{n+1}) \mathbf{n}_h^{n+1} \mathbf{w} dS - \int_{\Omega_h^{n+1}} \operatorname{div} \mathbf{v}_h^{n+1} q dx \\ & - \sum_{K \subset \Omega_h^{n+1}} \alpha_K \int_K \left(\frac{\mathbf{v}_h^{n+1} - \mathbf{v}_h^{n+1/2}}{\tau^n} + \nabla p_h^{n+1} - \mathbf{f} \right) \cdot \nabla q dx = 0, \end{aligned} \quad (19)$$

for all \mathbf{w} and q the velocity and pressure test functions, compatible with the boundary conditions on $\partial\Lambda$.

The restriction of the continuous piecewise linear approximation of the velocity \mathbf{v}_h^{n+1} at the center of each cells C_{ijk} permits to obtain the values \mathbf{v}_{ijk}^{n+1} on the structured grid for the next time step.

5 Numerical Results

Numerical results in the frame of mold filling have been presented in [5,13,14]. Here simulations involving surface tension effects are presented to validate the improvement of our model. The results are presented for a wide range of Reynolds and Capillary numbers, defined by $Re = \frac{h |\mathbf{v}| \rho}{\mu}$ and $Ca = \frac{\mu |\mathbf{v}|}{\sigma}$, where ρ is the density of the liquid, μ is the viscosity, $|\mathbf{v}|$ is the norm of the typical velocity, σ is the surface tension coefficient and h denotes the characteristic local distance, typically given by the mesh size. In the following simulations the ranges for the Reynolds and Capillary numbers are approximately $Re \simeq 10^0 - 10^4$ and $Ca \simeq 10^{-3} - 10^0$. Results for higher Reynolds

numbers ($Re \simeq 10^3 - 10^6$) and without surface tension have been presented in [5].

All the computations were performed on a computer with single processor Pentium Xeon 2.8 GHz CPU, 3 Gb Memory and running under Linux operating system.

5.1 Convergence Results

The test case of a stationary circular droplet of liquid lying in a square in the absence of gravity field is first considered. The radius of the droplet is $\sqrt{0.001}$ and the size of the square is 0.1×0.1 . Theoretical signed curvature is constant and equal to -31.62 on the boundary of the liquid domain. Several finite element meshes are considered: regular structured grids of squares, each square being divided in four triangles and unstructured (isotropic) meshes. Table 1 shows the relative error (in percent) on the curvature for several mesh sizes h and smoothing parameters ε .

If $\varepsilon \rightarrow 0$, the approximations of the derivatives of the characteristic function are not accurate. On the other hand, taking a large value of ε leads to an inaccurate approximation of the curvature (numerical diffusion). According to Tab. 1, a constant minimal value $\varepsilon = 0.05$ can be chosen, independently of the mesh size. This value ensures approximately one percent of error on the computation of the curvature for reasonable mesh sizes.

The convergence of the approximation of the curvature is discussed with fixed ε . Structured finite element meshes of squares are considered first from 40×40 squares to 400×400 squares, each square being divided in four triangles. The size of the cells of the structured mesh used for advection step is approximately 5 to 10 times smaller than the size of the finite elements, see [13,14]. Figure 5 illustrates the convergence of the approximation of the curvature when the mesh size tends to zero for $\varepsilon = 0.05$. The convergence order is $\mathcal{O}(h)$. Similar results are obtained with unstructured (isotropic) meshes, with the same order of convergence for the approximation of the curvature.

Since the time splitting algorithm presented in Sect. 3 is an order one algorithm (see also [13,14] for a numerical verification without taking into account the compressible gas), the aim of this article is not to increase the convergence order for the approximation of the curvature, even if the choice of the smoothing parameter ε in function of h could permit to obtain a better convergence order [32].

In the case of this stationary droplet, the numerical simulation introduces spurious velocities around the interface due to the imposition of surface tension

forces. Since the real physical velocity is identically zero, these velocities are often called *spurious currents* and their amplitude is widely discussed in the literature [3,21,23], in function of the ratio between the surface tension forces, *i.e.* $\sigma\kappa$, and the viscosity of the fluid, *i.e.* μ or in function of the Reynolds and Capillary numbers. In Fig. 6, the maximal amplitude of the spurious currents is given after five time steps ($\tau = 0.001$) for different mesh sizes. The ratio between surface tension forces and the viscosity is $\sigma\kappa/\mu \simeq 233.3$ and the Reynolds and Capillary numbers are respectively $Re \simeq 1.0$ and $Ca \simeq 0.0015$. Meshes are structured. The coarser finite element mesh is composed by 6400 elements (40×40 squares, each divided in four triangles) with 120×120 cells, the middle mesh is composed by 80×80 squares with 240×240 cells, while the finer mesh is composed by 120×120 squares divided in triangles with 360×360 cells. Results compare well for instance with [32] but are slightly less accurate than methods that reconstruct a very fine approximation of the interface, see *e.g.* [21].

In the following paragraphs, the efficiency and robustness of our method is illustrated on various examples.

5.2 Bubbles and Droplets Simulations

Deformed droplets have been widely treated in the literature [3,15,23,29]. Here we consider first an initially oval droplet in the absence of gravity forces. Since the surface tension forces are more important in the extremities where the curvature is larger, the shape of the droplet tends to become a circle. In our case, the viscosity is given by $\mu = 1$ kg/(ms), while the density is $\rho = 1000$ kg/m³. The surface tension coefficient is $\sigma = 7.038$ N/m. The external pressure of the surrounding gas is neglected. The initial liquid domain is given by

$$\Omega_0 = \left\{ (x, y) \in \mathbb{R}^2 : \left(\frac{x-4}{2} \right)^2 + \left(\frac{y-4}{3} \right)^2 \leq 1 \right\} .$$

A coarse structured mesh is made out of 20×20 squares, each divided in 4 triangles. A middle mesh (40×40 squares) and a fine mesh (80×80 squares) are also considered. The regular grid of small cells is constituted respectively by 500×500 , 1000×1000 and 2000×2000 cells. The time step is $\tau = 0.1$, 0.05 and 0.025 s respectively. The orders of magnitude for the Reynolds number and Capillary number are approximately $Re \simeq 1.0$ and $Ca \simeq 0.0029$. Since the liquid is a viscous liquid, the amplitude of the oscillations decreases with time and the oval droplet becomes a circle after some oscillations. The period of oscillations for droplets has been extensively discussed in the literature (see for instance [2] and references therein). According to [8,20], the period ξ of the first mode of oscillations of a cylindrical droplet of density ρ into the vacuum

is given by:

$$\xi^2 = \frac{6\sigma}{\rho a^3} , \quad (20)$$

where a is the radius of the circle in equilibrium. This approximation does not take into account the viscous effects. Nevertheless, for large droplets of low viscosity liquids (see [2,12]) such as this case, the viscous corrections have been proved to be negligible and (20) holds.

For $a = 2.45$, $\rho = 1000$ and $\sigma = 7.038$, the theoretical value of the time to make one complete oscillation is $2\pi/\xi \simeq 0.1173$ s. The period of the computed droplet oscillation is determined by studying the position of one extreme point along one axis of the droplet. The observed values for the period of oscillation in the simulations are respectively 0.130 s. for the coarser mesh, 0.122 s. for the middle mesh and 0.115 s. for the finer mesh. This shows that the diffusion of the algorithm decreases with the mesh size, with order one, see Fig. 7.

Similar results may be obtained in the three dimensional case. For instance let $\Omega_0 = \left\{ (x, y, z) \in \mathbb{R}^3 : \left(\frac{x-0.05}{0.8} \right)^2 + \left(\frac{y-0.05}{1.8} \right)^2 + \left(\frac{z-0.05}{0.8} \right)^2 \leq (0.025)^2 \right\}$. Figure 8 illustrates the position of the liquid-gas interface at different times for a coarse finite element mesh made out of 96'000 tetrahedrons. The CPU time used for this computation is approximately 10 hours to achieve 400 time steps.

Let us consider now the rising of a bubble, see Fig. 1. Consider a bubble of gas initially at the bottom of a cylinder filled with liquid. Under gravity forces, the bubble rises until reaching the top of the cylinder. The physical constants are $\mu = 0.01$ kg/(ms), $\rho = 1000$ kg/m³ and $\sigma = 0.0738$ N/m. Consider first the two-dimensional case. The dimensions of the cylinder are 0.1 m \times 0.05 m. The Reynolds and Capillary numbers are respectively $Re \simeq 80$ and $Ca \simeq 0.11$. Three structured finite element meshes are considered. The coarse mesh is made out of 2576 nodes and 5000 elements, the middle mesh is made out of 10151 nodes and 20000 elements and the fine mesh is made out of 22726 nodes and 45000 elements. The size of the cells of the structured mesh used for advection step is approximately 5 to 10 times smaller than the size of the finite elements and the time step is chosen such that the CFL number is approximately one. The smoothing parameter is $\varepsilon = 0.005$. Figure 9 illustrates the liquid-gas interface at different times for different mesh sizes. The convergence when the mesh size and time step tend to zero appears clearly thanks to surface tension effects.

Similar results may be obtained in three space dimensions and are illustrated in Fig. 10 for a mesh made out of 115'200 tetrahedrons. The CPU time for this computation is approximately 20 hours to achieve 1000 time steps. Most of the CPU time is used to solve the Stokes problem in the liquid domain.

5.3 Droplet splashing

The splashing of a droplet of liquid falling in the presence of gravity field onto a thin layer of the same liquid at rest is considered in two space dimensions (see also [10]). The cavity is the $0.1\text{ m} \times 0.1\text{ m}$ square. External forces are only gravity forces. The droplet has initial velocity $\mathbf{v}_0 = -2\text{ m/s}$ along vertical axis and falls from 0.0625 m . The initial radius of the bubble is 0.007 m and the height of the thin layer of liquid is 0.02 m . Physical parameters are $\mu = 0.05\text{ kg/(ms)}$, $\rho = 1000\text{ kg/m}^3$ and $\sigma = 0.0738\text{ Nm}^{-1}$. Numerical results are presented for a structured mesh of 80×80 squares and the time step is $\tau = 0.001\text{ s}$. The final time is $T = 0.4\text{ s}$. The smoothing parameter is $\varepsilon = 0.05$. The Reynolds number is approximately $Re \simeq 40$ and the Capillary number is $Ca \simeq 1.35$. Slip boundary conditions are enforced on the lateral walls, while no slip boundary conditions are enforced at the bottom of the cavity. The position of the free boundary is illustrated in Fig. 11 for various times and shows the formation of small splashing droplets.

5.4 Filling of a Plate

Generally, surface tension is not the leading effect in mold filling applications, due to high Reynolds numbers. A filling example is presented here to validate our extended model in the framework of mold filling. Consider here the filling of a plate. The mold is included in a $0.1\text{ m} \times 0.1\text{ m}$ -rectangular domain, whose thickness is 0.05 m . Liquid ($\rho = 1000\text{ kg/m}^3$ and $\mu = 0.01\text{ kg/(ms)}$) is injected from the bottom at vertical velocity 16 m/s through a small inlet. The experiment is three-dimensional, but the small thickness of the mold allows to perform simulations in two dimensions of space. Thanks to the symmetry of the problem, the simulation covers one-half of the physical domain and slip boundary conditions are imposed on the symmetry axis. The finite element mesh is made out of 1960 nodes, while the structured grid is made out of 60'000 cells. The Reynolds number is $Re \simeq 10^4$. Two different surface tension coefficients are selected ($\sigma = 0.0738\text{ N/m}$ and $\sigma = 7.38\text{ N/m}$) giving Capillary numbers of $Ca \simeq 2.17$ or $Ca \simeq 0.0217$ respectively.

In Fig. 12, numerical results are presented for different values of σ when the cavity is initially filled with an ideal gas at atmospheric pressure and compared to experiments [24].

When comparing numerical results to experimental ones, we can observe the absence of the rolling at the front of the jet in the simulations and a large difference (blurring) in the shape of the front of the flow before hitting the opposite wall. These differences are probably due to inexact slip boundary

conditions, especially at the entrance of the cavity, where there is a large friction between the wall and the liquid. These boundary conditions are enforced to avoid the boundary layers effects that would appear with the friction of the liquid against the walls at the entrance of the cavity and would need extremely fine layered meshes along the boundary of the cavity. The second reason is the absence of a sophisticated turbulence model in our model that would allow to take into account the turbulent character of the flow that is not well simulated with our simple turbulent viscosity model.

In both cases, the introduction of surface tension does not help to improve the simulation for such turbulent flows, but this example shows the robustness of the surface tension computations in the framework of mold filling.

6 Conclusion

A numerical model for the simulation of free surface flows with surface tension involving a compressible gas and an incompressible liquid has been presented. The characteristic function of the liquid domain is used to describe the interface. The unknowns are velocity and pressure in the liquid and constant pressure in each connected component of gas surrounded by the liquid. A splitting algorithm is used to decouple physical phenomena. The surface tension effects are taken into account in a variational form that permits to avoid the need of a very accurate reconstruction of the interface. Numerical results show on various examples the efficiency and robustness of the method.

Acknowledgements

The author wishes to thank Dr Marco Picasso and Prof. Jacques Rappaz, Institut d'Analyse et Calcul Scientifique, Ecole Polytechnique Fédérale de Lausanne, CH-1015 Lausanne for fruitful remarks and discussions and Dr Vincent Maronnier, Calcom Company, ESI group, Parc Scientifique, CH-1015 Lausanne for implementation support. The Calcom Company is acknowledged for kindly providing the CalcoSoftTM software.

References

- [1] E. Aulisa, S. Manservigi, and R. Scardovelli. A Mixed Markers and Volume-of-Fluid Method for the Reconstruction and Advection of Interfaces in Two-Phase and Free-Boundary Flows. *J. Comp. Phys.*, 188:611–639, 2003.

- [2] E. Becker, W. J. Hiller, and T. A. Kowalewski. Experimental and Theoretical Investigation of Large Amplitude Oscillations of Liquid Droplets. *J. Fluid Mech.*, 231:189–210, 1991.
- [3] J. U. Brackbill, D. B. Kothe, and C. Zemach. A Continuum Method for Modeling Surface Tension. *J. Comp. Phys.*, 100:335–354, 1992.
- [4] J.W. Bullard, E.J. Garboczi, W.C. Carter, and E.R. Fuller Jr. Numerical Methods for Computing Interfacial Mean Curvature. *Computational Materials Science*, 4:103–116, 1995.
- [5] A. Caboussat, M. Picasso, and J. Rappaz. Numerical Simulation of Free Surface Incompressible Liquid Flows Surrounded by Compressible Gas. *J. Comput. Phys.*, 203(2):626–649, 2005.
- [6] A. J. Chorin. Curvature and Solidification. *J. Comp. Phys.*, 58:472–490, 1985.
- [7] S. Dufour and D. Pelletier. Computations of Multiphase Flows with Surface Tension using Adaptive Finite Element Methods. In *Proceedings of the 37th AIAA Aerospace Sciences Meeting and Exhibit, Reno*, number 99-0544 in AIAA Paper, 1999.
- [8] D. E. Fyfe, E. S. Oran, and M. J. Fritts. Surface Tension and Viscosity with Lagrangian Hydrodynamics on a Triangular Mesh. *J. Comp. Phys.*, 76:349–384, 1988.
- [9] M. Gerhardt, H. Schuster, and J. J. Tyson. A Cellular Automaton Model of Excitable Media: II Curvature, Dispersion, Rotating Waves and Meandering Waves. *Physica D*, 46:392–415, 1990.
- [10] Ch. Josserand and S. Zaleski. Droplet Splashing on a Thin Liquid Film. *Phys. Fluids*, 15(6):1650–1657, 2003.
- [11] M. Kang, R. P. Fedkiw, and X.-D. Liu. A Boundary Condition Capturing Method for Multiphase Incompressible Flow. *Journal of Scientific Computing*, 15:323–360, 2000.
- [12] H. Lamb. *Hydrodynamics*. Dover, 6th edition, 1945.
- [13] V. Maronnier, M. Picasso, and J. Rappaz. Numerical Simulation of Free Surface Flows. *J. Comput. Phys.*, 155:439–455, 1999.
- [14] V. Maronnier, M. Picasso, and J. Rappaz. Numerical Simulation of Three Dimensional Free Surface Flows. *Int. J. Num. Meth. Fluids*, 42(7):697–716, 2003.
- [15] M. Meier, G. Yadigaroglu, and B. L. Smith. A Novel Technique for Including Surface Tension in PLIC-VOF Methods. *European Journal of Mechanics B - Fluids*, 21:61–73, 2002.
- [16] W.F. Noh and P. Woodward. *SLIC (Simple Line Interface Calculation)*, volume 59 of *Lectures Notes in Physics*, pages 330–340. Springer-Verlag, 1976.

- [17] S. Osher and R. P. Fedkiw. Level Set Methods : An Overview and Some Recent Results. *J. Comp. Phys.*, 169:463–502, 2001.
- [18] S. Popinet and S. Zaleski. A Front-Tracking Algorithm for Accurate Representation of Surface Tension. *Int. J. Numer. Meth. Fluids*, 30:777–793, 1999.
- [19] A.R.M. Primo, L.C. Wrobel, and H. Power. Low Reynolds Number Deformation of Viscous Drops in a Bounded Flow Region under Surface Tension. *Mathematical and Computer Modelling*, 31:99–118, 2000.
- [20] J. W. S. Rayleigh. On the Capillary Phenomena of Jets. *Proc. R. Soc. Lond.*, 29:71–97, 1896.
- [21] Y. Renardy and M. Renardy. PROST : A Parabolic Reconstruction of Surface Tension for the Volume-Of-Fluid Method. *J. Comp. Phys.*, 183:400–421, 2002.
- [22] W.J. Rider and D.B. Kothe. Reconstructing Volume Tracking. *J. Comp. Phys.*, 141:112–152, 1998.
- [23] R. Scardovelli and S. Zaleski. Direct Numerical Simulation of Free Surface and Interfacial Flows. *Annual Review of Fluid Mechanics*, 31:567–603, 1999.
- [24] M. Schmid and F. Klein. Einfluß der Wandreibung auf das Füllverhalten Dünnere Platten. *Preprint, Steinbeis Transferzentrum, Fachhochschule Aachen*, 1996.
- [25] J.A. Sethian. *Level Set Methods, Evolving Interfaces in Geometry, Fluid Mechanics, Computer Vision, and Material Science*. Monographs on Applied and Computational Mathematics. Cambridge University Press, 1996.
- [26] M. J. Shelley, F.-R. Tian, and K. Wlodarski. Hele-Shaw Flow and Pattern Formation in a Time-Dependent Gap. *Nonlinearity*, 10:1471–1495, 1997.
- [27] A. Smolianski, H. Haario, and P. Luukka. Computational Study of Bubble Dynamics. *submitted to Comput. and Fluids.*, 2003.
- [28] M. Sussman and E. G. Puckett. A Coupled Level Set and Volume-of-Fluid Method for Computing 3D and Axisymmetric Incompressible Two-Phase Flows. *J. Comp. Phys.*, 162:301–337, 2000.
- [29] D.J. Torres and J.U.Brackbill. The Point-Set Method: Front-Tracking without Connectivity. *J. Comp. Phys.*, 165:620–644, 2000.
- [30] G. Tryggvason, B. Bunner, A. Esmaeeli, D. Juric, N. Al-Rawahi, W. Tauber, J. Han, S. Nas, and Y.-J. Jan. A Front-Tracking Method for the Computations of Multiphase Flows. *J. Comp. Phys.*, 169:708–759, 2001.
- [31] S.P. van der Pijl, A. Segal, and C. Vuik. A Mass-Conserving Level-Set (MCLS) Method for Modeling of Multi-Phase Flows. Technical Report 03-03, Delft University of Technology, 2003.

- [32] M. W. Williams, D. B. Kothe, and E. G. Puckett. Accuracy and Convergence of Continuum Surface Tension Models. In Cambridge Cambridge Univ. Press, editor, *Fluid Dynamics at Interfaces*, pages 294–305. Fluid Dynamics at Interfaces, Gainesville, FL, 1998, 1999.

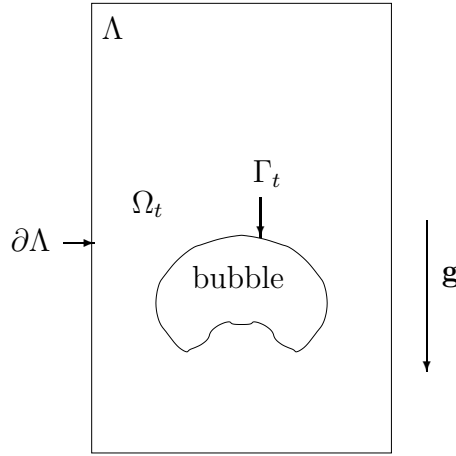


Fig. 1. Rising of a bubble of air under gravity forces in a cavity Λ filled with water.

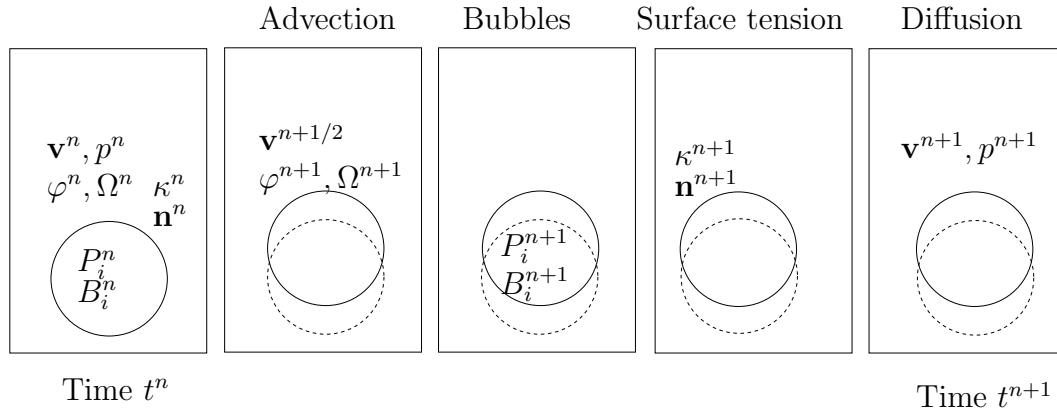


Fig. 2. The splitting algorithm (from left to right). Two advection problems are solved to determine the new approximation of the characteristic function φ^{n+1} , the new liquid domain Ω^{n+1} and the predicted velocity $\mathbf{v}^{n+1/2}$. Then a constant pressure P_i^{n+1} is computed in each bubble B_i^{n+1} . The curvature κ^{n+1} and the normal vector \mathbf{n}^{n+1} are then obtained on the liquid-gas interface. Finally, a generalized Stokes problem is solved to obtain the velocity \mathbf{v}^{n+1} and the pressure p^{n+1} in the new liquid domain Ω^{n+1} , taking into account the pressure P_i^{n+1} and curvature κ^{n+1} on the liquid-gas interface.

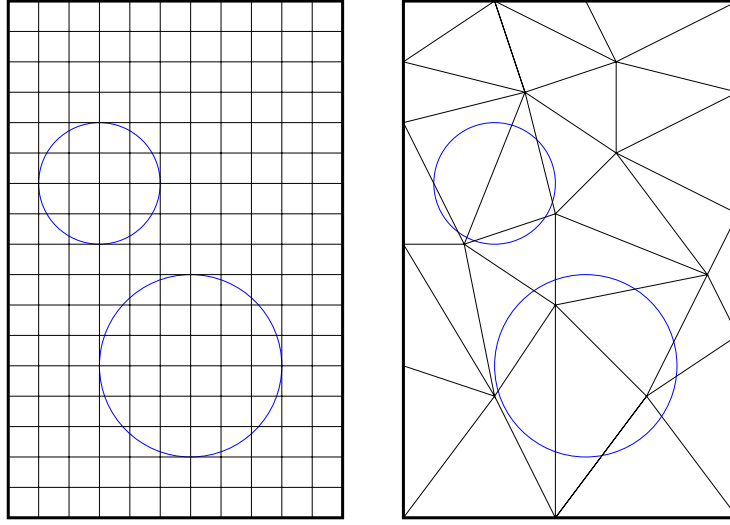


Fig. 3. Two grids method in the two-dimensional case: structured grid of small square cells (left) and unstructured finite element mesh of triangles (right).

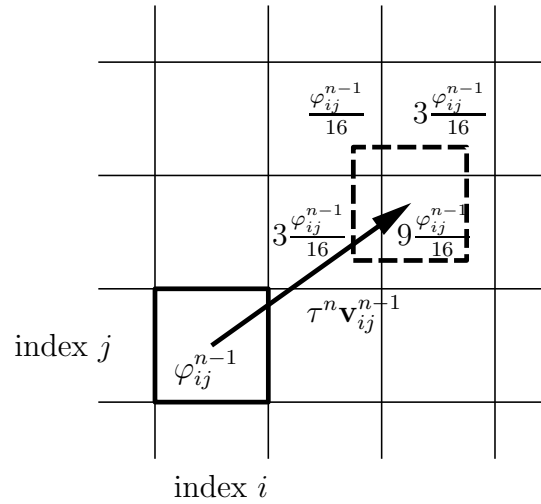


Fig. 4. An example of two dimensional advection of φ_{ij}^n by $\tau^{n+1} \mathbf{v}_{ij}^n$, and projection on the grid. The advected cell is represented by the dashed lines. The four cells containing the advected cell receive a fraction of φ_{ij}^n , according to the position of the advected cell.

| $\varepsilon \backslash h$ | 0.0025 | 0.0016 | 0.00125 | 0.001 | 0.0008 |
|----------------------------|--------|--------|---------|-------|--------|
| 0.5 | 3.85 | 1.51 | 1.45 | 1.10 | 0.85 |
| 0.1 | 3.85 | 1.42 | 1.49 | 1.10 | 0.85 |
| 0.05 | 3.82 | 1.42 | 1.42 | 1.10 | 0.85 |
| 0.01 | 4.14 | 1.48 | 1.45 | 1.12 | 0.89 |
| 0.005 | 8.03 | 1.67 | 1.49 | 1.15 | 1.04 |

Table 1

Circular droplet case: smoothing of volume fraction of liquid. Values of the maximal relative error (in percent) on the curvature of the circular droplet function of parameter ε and of mesh size h .

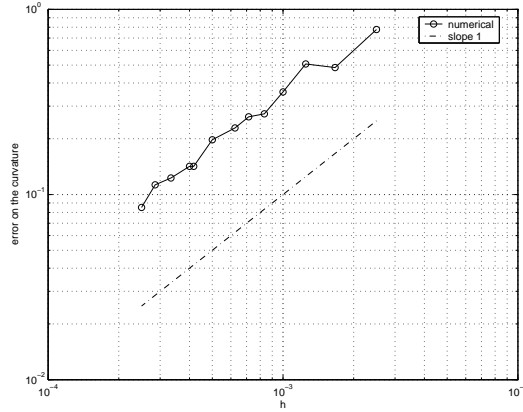


Fig. 5. Circular droplet test case: convergence error for the approximation of the curvature.

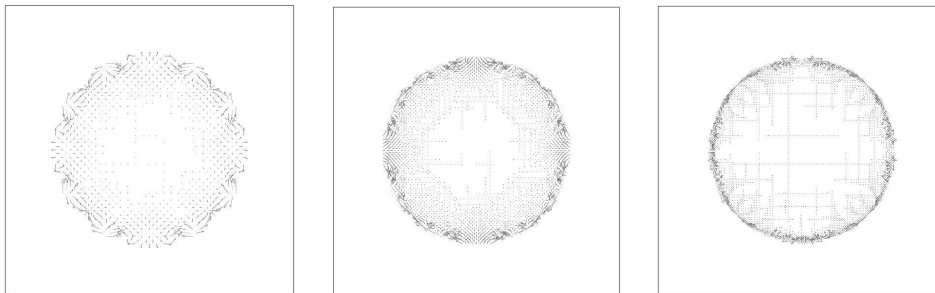


Fig. 6. Spurious currents: Representation of the spurious velocities on a circle shape for coarse mesh (left, $h = 0.0025$, $|\mathbf{v}|_{\max} = 0.0057$ m/s), middle mesh (center, $h = 0.00125$, $|\mathbf{v}|_{\max} = 0.0078$ m/s) and fine mesh (right, $h = 0.00083$, $|\mathbf{v}|_{\max} = 0.0109$ m/s).

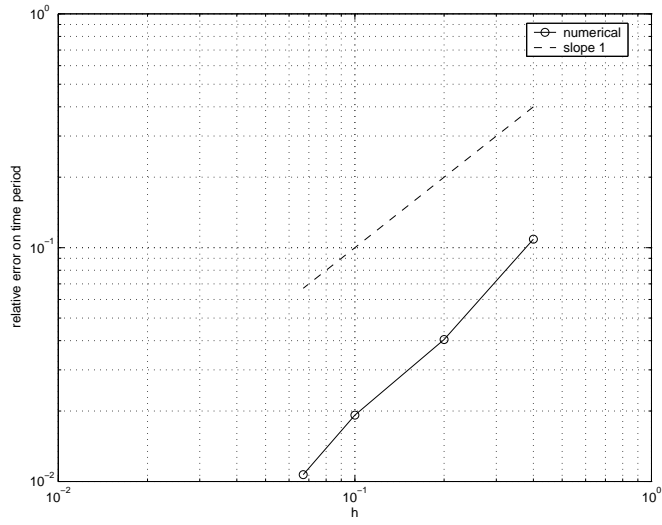


Fig. 7. Oscillating droplet: Log-scale plot of the relative error on the time period for the first oscillation of the droplet.

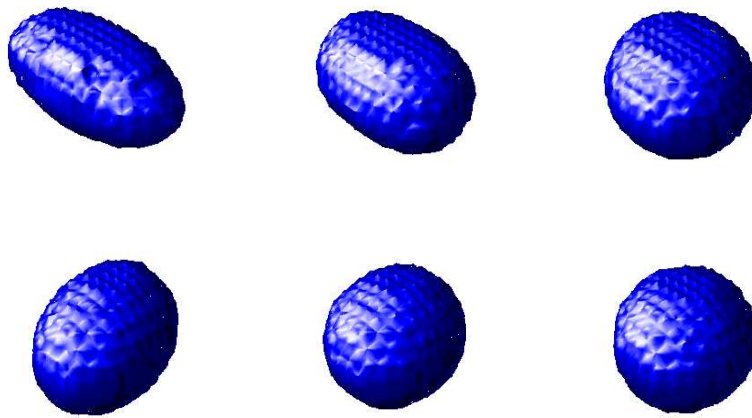


Fig. 8. Three-dimensional oval droplet. Representation of the liquid-gas interface at various times (from left to right, top to bottom $t = 0.15, 0.30, 0.44, 0.74, 1.2$ and 1.5 s.)

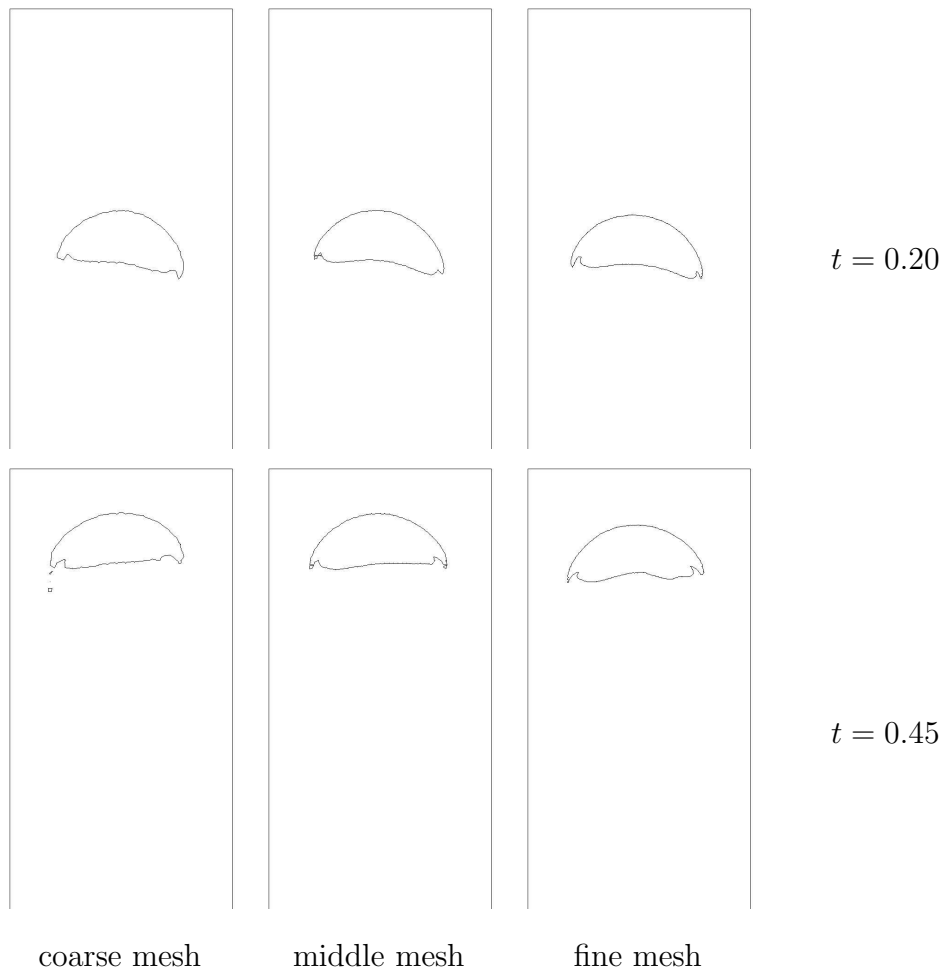


Fig. 9. Rising Bubble: results for $\sigma = 0.0738 \text{ Nm}^{-1}$ and several mesh sizes. Position of the free surface at times $t = 0.2 \text{ s}$ (first row) and $t = 0.45 \text{ s}$ (second row). Left: coarse mesh, middle: middle mesh and right: fine mesh.

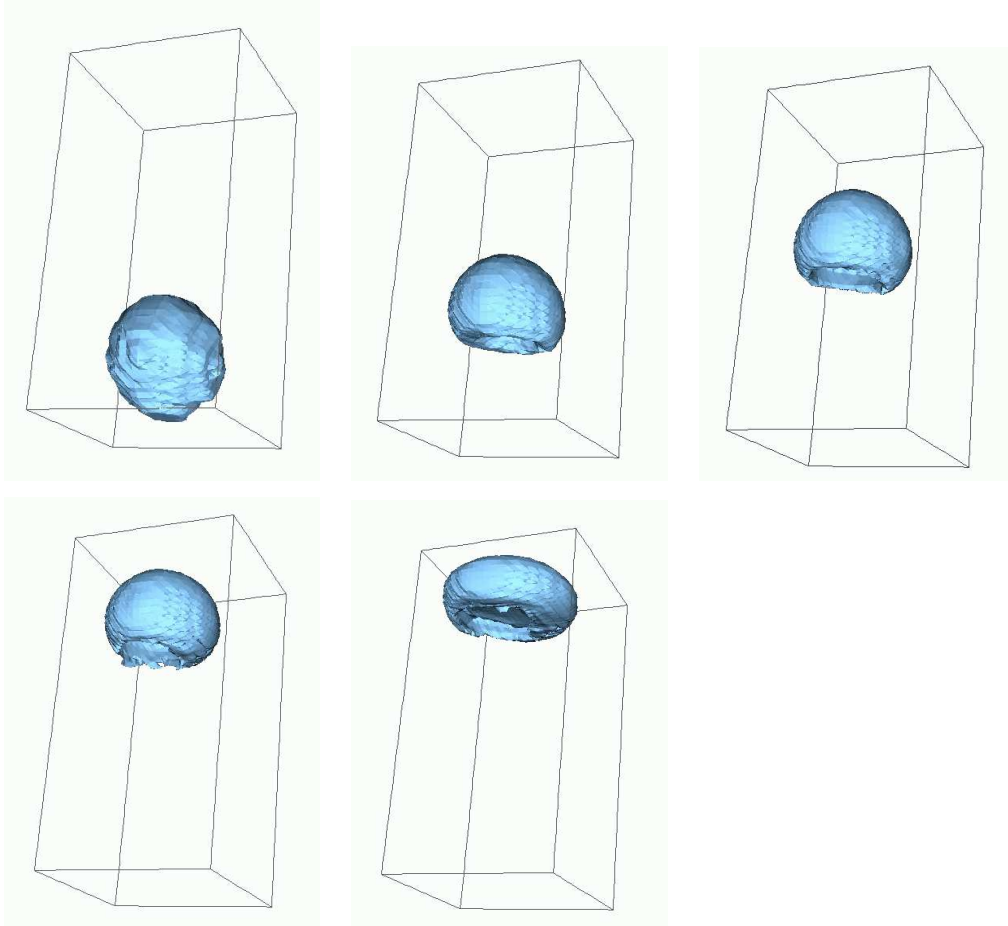


Fig. 10. Rising Bubble: three-dimensional results for $\sigma = 0.0738 \text{ Nm}^{-1}$. Representation of the gas domain at times $t = 0.0, 0.25, 0.5, 0.75$ and 1 s. (left to right, top to bottom)

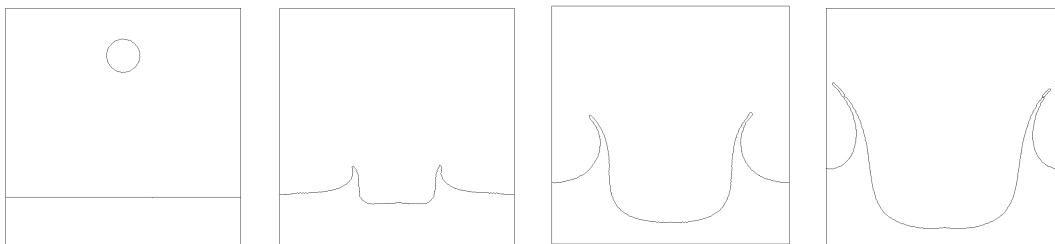


Fig. 11. Droplet splashing on a thin layer of liquid. Position of the liquid gas interface at times $t = 0, 0.04, 0.06$ and 0.08 s.

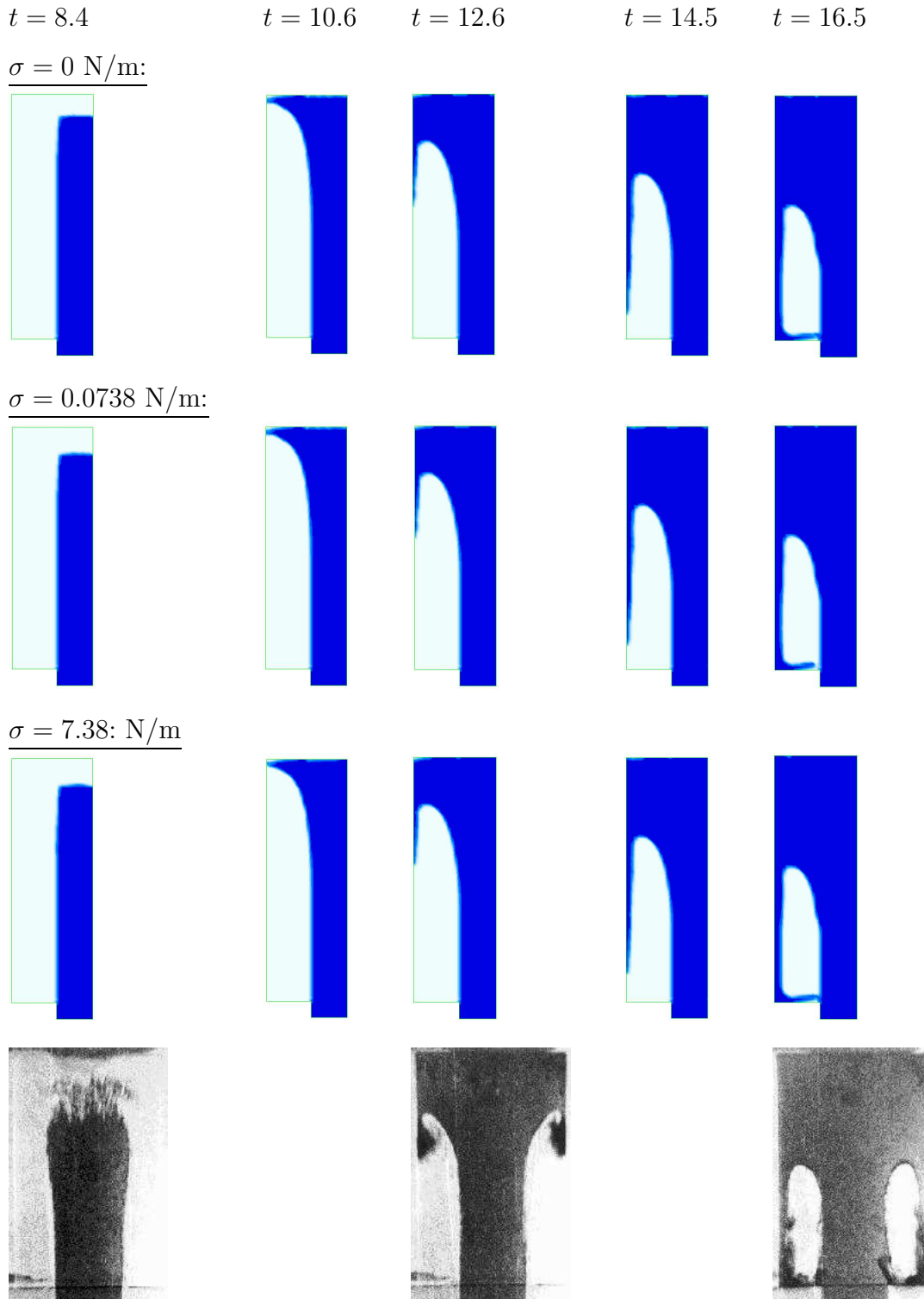


Fig. 12. A mold filling example: numerical results at times 8.4, 10.6, 12.6, 14.5 and 16.5 ms: first row: without surface tension, second row: with surface tension $\sigma = 0.0738 \text{ N/m}$, third row: with surface tension $\sigma = 7.38 \text{ N/m}$ and fourth row: experiment [24] at times 8.4, 12.6 and 16.5 ms.